

Next-to-leading-order predictions for $D^{*\pm}$ plus jet photoproduction at DESY HERA

Gudrun Heinrich

*. Institut für Theoretische Physik, Universität Hamburg,
Luruper Chaussee 149, 22761 Hamburg, Germany*

Bernd A. Kniehl*

*Max-Planck-Institut für Physik (Werner-Heisenberg-Institut),
Föhringer Ring 6, 80805 Munich, Germany*

Abstract

We study the photoproduction of a $D^{*\pm}$ meson in association with a hadron jet at next-to-leading order in the parton model of QCD with non-perturbative fragmentation functions extracted from LEP1 data of e^+e^- annihilation. The transverse-momentum and rapidity distributions recently measured at DESY HERA in various kinematic ranges nicely agree with our theoretical predictions. This provides a useful test of the universality and the scaling violations of the fragmentation functions predicted by the factorization theorem. These comparisons also illustrate the significance of the charm component in the resolved photon. This is elaborated by investigating the cross-section distributions in x_{obs}^γ and $\cos \theta^*$.

PACS numbers: 12.38.Bx, 12.39.St, 13.60.Le, 14.40.Lb

*Permanent address: II. Institut für Theoretische Physik, Universität Hamburg, Luruper Chaussee 149, 22761 Hamburg, Germany

I. INTRODUCTION

Heavy-flavor production has always been an important testing ground for quantum chromodynamics (QCD), one of the reasons being that it addresses the problem of where to draw the dividing line between perturbative and non-perturbative aspects. The photoproduction of open charm is particularly interesting because it also allows valuable insights into the partonic structure of the photon. Results on inclusive $D^{*\pm}$ photoproduction from the H1 [1] and ZEUS [2, 3] Collaborations at the DESY ep collider HERA have been compared to leading-order (LO) and next-to-leading order (NLO) calculations [4, 5, 6]. More recently, data on the photoproduction of a $D^{*\pm}$ meson in association with a hadron jet have also become available [3, 7, 8, 9, 10].

Concerning the theoretical treatment of open heavy-flavor production, several approaches have been followed in the literature. The QCD-improved parton model implemented in the modified minimal-subtraction ($\overline{\text{MS}}$) renormalization and factorization scheme and endowed with non-perturbative fragmentation functions (FFs), which proved itself so convincingly for light-hadron inclusive production [11], also provides an ideal theoretical framework for a coherent global analysis of D - [6] and B -meson data [12], provided that $\mu \gg m_Q$, where μ is the energy scale characteristic for the respective production process and $Q = c, b$. Then, at LO (NLO), the dominant logarithmic terms, of the form $\alpha_s^n \ln^n (\mu^2/m_Q^2)$ ($\alpha_s^{n+1} \ln^n (\mu^2/m_Q^2)$) with $n = 1, 2, \dots$, where α_s is the strong-coupling constant, are properly resummed to all orders by the time-like Dokshitzer-Gribov-Lipatov-Altarelli-Parisi (DGLAP) [13] evolution, while power terms of the form $(m_Q^2/\mu^2)^n$ are negligibly small and can be safely neglected. In this *massless-quark scheme* or *zero-mass variable-flavour-number scheme* (ZMVFNS), which is sometimes improperly referred to as *NLL approximation* [39], the Q quark is treated as massless and appears as an active parton in the incoming hadron or photon, having a non-perturbative parton density function (PDF). The criterion $\mu \gg m_Q$ is certainly satisfied for e^+e^- annihilation on the Z -boson resonance, and for the photo-, lepto-, and hadroproduction of D and B hadrons with transverse momenta $p_T \gg m_Q$. Furthermore, the universality of the FFs is guaranteed by the factorization theorem [14], which entitles us to transfer information on how charm and bottom quarks hadronize to D and B hadrons, respectively, in a well-defined quantitative way from e^+e^- annihilation, where the measurements are usually most precise, to other kinds of experiments, such as photo-, lepto-, and hadroproduction. In

Refs. [6, 12], the distributions in the scaled D - and B -hadron energy $x = 2E/\sqrt{s}$ measured at LEP1 were fitted at LO and NLO in the ZMVFNS using, among others, the ansatz by Peterson *et al.* [15] for the $c \rightarrow D$ and $b \rightarrow B$ FFs at the starting scale $\mu_0 = 2m_Q$. In the $D^{*\pm}$ (B^+/B^0) case, the ε parameter was found to be $\varepsilon_c = 0.0851$ and 0.116 [6] ($\varepsilon_b = 0.0126$ and 0.0198 [12]) at LO and NLO, respectively. We emphasize that the value of ε carries no meaning by itself, but it depends on the underlying theory for the description of the fragmentation process, in particular, on the choice of the starting scale μ_0 , on whether the analysis is performed in LO or NLO, and on how the final-state collinear singularities are factorized in NLO. An alternative to the ZMVFNS with purely non-perturbative FFs is to decompose the FFs into a perturbative component, the so-called *perturbative FFs* (PFFs) [16], and a non-perturbative component [5, 17].

In the traditional *massive-quark scheme* or *fixed-flavour-number scheme* (FFNS), the Q quark is treated in the on-mass-shell renormalization scheme, as if it were a massive lepton in triplicate, and it only appears in the final state, but not as an active parton inside the incoming hadron or photon. There are no collinear singularities associated with the outgoing Q -quark lines that need to be subtracted and absorbed into FFs. This scheme breaks down for $p_T \gg m_Q$ because of would-be collinear singularities of the form $\alpha_s \ln(p_T^2/m_Q^2)$, which are not resummed. However, this scheme allows one to calculate a total cross section, which is infeasible in the ZMVFNS. Quantitative comparisons of the ZMVFNS and the FFNS for photoproduction in ep and $\gamma\gamma$ collisions may be found in Refs. [18] and [19], respectively.

A rigorous theoretical framework that retains the full finite- m_Q effects while preserving the indispensable virtues of the factorization theorem, namely the universality and the DGLAP [13] scaling violations of the FFs, is provided by the *general-mass variable-flavour-number scheme* (GMVFNS) [14, 20]. In a nutshell, this procedure consists in explicitly performing the $m_Q \rightarrow 0$ limit of the FFNS result, comparing the outcome, term by term, with the ZMVFNS result in the $\overline{\text{MS}}$ scheme, and subtracting the difference terms from the FFNS result. Owing to the factorization theorem [14], the hard-scattering cross sections thus obtained can then be convoluted with non-perturbative D - and B -hadron FFs extracted from LEP1 data using the pure $\overline{\text{MS}}$ scheme [6, 12]. This is consistent because the finite- m_Q terms omitted in Refs. [6, 12] are relatively small, of order m_Q^2/m_Z^2 . The impact of finite- m_Q terms on the proton PDFs was recently assessed by the CTEQ Collaboration [21]. In this connection, we should also mention the so-called *fixed-order next-to-leading-logarithm*

(FONLL) scheme [22], in which the ordinary result in the FFNS and a suitably subtracted result in a ZMVFNS with PFFs are linearly combined using a certain weight function [22]. The conceptual merits of the GMVFNS and the FONLL are reviewed in Ref. [23].

The GMVFNS was recently implemented for direct [24] and single-resolved [25] $\gamma\gamma$ collisions as well as for ep collisions with quasi-real photons [26]. In the case of $\gamma\gamma \rightarrow D^{*\pm} + X$ at LEP2, the inclusion of finite- m_c effects was found to reduce the cross section by approximately 20% (10%) at $p_T^D = 2m_c$ ($3m_c$) [24], *i.e.*, their magnitude is roughly $m_c^2/(p_T^D)^2$, as naively expected. From Refs. [24, 25, 26], we thus infer that finite- m_c effects play a significant role only at rather small p_T^D values, $p_T^D \lesssim 3$ GeV, so that the ZMVFNS should yield a good approximation in the kinematic range $p_T^D > 3$ GeV and $p_T^j > 6$ GeV considered in a very recent ZEUS analysis [9].

The article is organized as follows. In Sec. II, we give a short description of the method. In Sec. III, we present a numerical analysis of $D^{*\pm}$ plus jet associated photoproduction, where we also compare to preliminary ZEUS data [9]. Section IV contains the conclusions.

II. THEORETICAL FRAMEWORK

Using the massless scheme, we can rely on the factorization theorem and write the photoproduction cross section for $ep \rightarrow \gamma p \rightarrow D^{*\pm} + X$ as a convolution of the partonic cross section $\hat{\sigma}$ with the PDFs of the incident particles and the FFs for an outgoing parton fragmenting into a $D^{*\pm}$ meson. In this approach, the FFs are purely non-perturbative, universal, and subject to DGLAP [13] evolution. We have

$$d\sigma^{ep \rightarrow D^{*\pm} + X}(P_e, P_p, P_D) = \sum_{i,j,k} \int dx_e dx_p dz F_{i/e}(x_e, M_e) F_{j/p}(x_p, M_p) D_{D/k}(z, M_F) \times d\hat{\sigma}^{ij \rightarrow kX}(x_e P_e, x_p P_p, P_D/z, \mu, M_e, M_p, M_F), \quad (1)$$

where M_e and M_p are the initial-state factorization scales, M_F is the final-state factorization scale, and μ the renormalization scale. If a jet in addition to the $D^{*\pm}$ meson is detected, a measurement function defining the jet has to be included in Eq. (1). The sum $\sum_{i,j,k}$ runs over all partons, including quarks, gluons as well as photons, which can contribute if the energy of the subprocess is above their mass thresholds. Therefore, the charm quark also contributes as an incoming parton originating from the proton or the resolved photon.

At leading order, the subprocesses contributing to the partonic reaction $ij \rightarrow kX$ can be divided into two categories, corresponding to a direct or a resolved photon in the initial state. The direct photon corresponds to $i = \gamma$ in Eq. (1), with $F_{\gamma/e}$ approximated by the Weizsäcker-Williams formula for the spectrum of the quasi-real photons,

$$F_{\gamma/e}(y) = \frac{\alpha_{em}}{2\pi} \left[\frac{1 + (1-y)^2}{y} \ln \frac{Q_{\max}^2(1-y)}{m_e^2 y^2} - \frac{2(1-y)}{y} \right], \quad (2)$$

where α_{em} is Sommerfeld's fine-structure constant and Q_{\max}^2 is the maximum virtuality of the photon. On the other hand, the resolved photon participates in the hard interaction via its quark and gluon content. In this case, $F_{i/e}(x_e, M_e)$ is given by a convolution of the Weizsäcker-Williams spectrum with the photon PDFs as

$$F_{i/e}(x_e, M_e) = \int_0^1 dy dx_\gamma F_{\gamma/e}(y) F_{i/\gamma}(x_\gamma, M_e) \delta(yx_\gamma - x_e). \quad (3)$$

Typical examples of LO diagrams are depicted in Fig. 1.

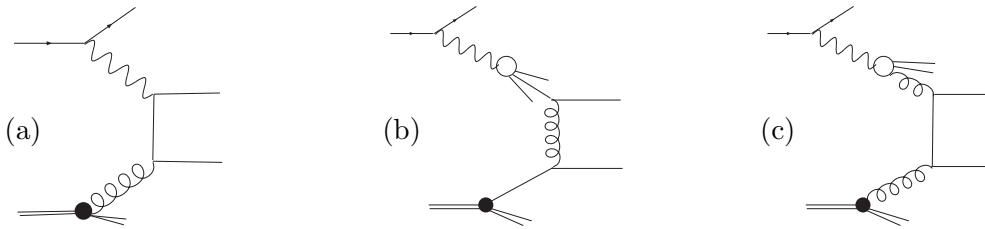


FIG. 1: Examples of LO diagrams involving (a) direct photons or (b) the quark or (c) gluon components of resolved photons.

At NLO, an additional real or virtual parton can be radiated in the hard interaction. Representative examples of NLO diagrams are shown in Fig. 2. As the partons are massless, this leads to soft and collinear singularities. The soft singularities cancel between the real and the virtual corrections, while the collinear ones are absorbed into the PDFs or FFs. For example, the collinear singularities appearing at NLO if the incident photon splits into a collinear $q\bar{q}$ pair are absorbed into the PDF $F_{q/\gamma}(x_\gamma, M_e)$ at the factorization scale M_e . Thus the direct- and resolved-photon contributions separately exhibit strong dependences on M_e , which cancel out only in their sum, up to terms which are formally beyond NLO. Therefore, it has to be stressed that, at NLO, only the sum of the two contributions carries a physical meaning. Technically, the infrared divergences have been isolated using a combination of

the phase-space-slicing [27] and the subtraction [28] methods. A more detailed description of the calculation can be found in Refs. [29, 30] and will not be repeated here. The matrix elements have been calculated in Refs. [31] and are implemented in the computer program **EPHOX** [32], which can serve to calculate the photoproduction of a large- p_T hadron or photon together with an optional jet. The program is constructed as a partonic event generator, so that the total cross section as well as differential distributions can be easily obtained.

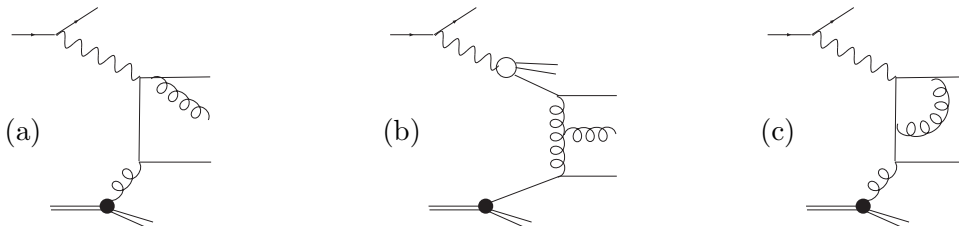


FIG. 2: Examples of NLO diagrams contributing to the real corrections in (a) direct and (b) resolved photoproduction, and (c) to the virtual corrections in direct photoproduction.

III. NUMERICAL RESULTS

We are now in a position to present our numerical analysis. We start by specifying our inputs and the kinematic situation. We work in the ZMVFNS with $n_f = 5$ massless quark flavors. For the PDFs of the proton, we take the MRST03 [33] set by Martin, Roberts, Stirling, and Thorne. For the PDFs of the photon, our default set is AFG04 [34] by Aurenche, Fontannaz, and Guillet, which is an updated version of the original AFG [35] parameterization. In contrast to the AFG [35] set, the AFG04 [34] set also contains a bottom-quark PDF. The AFG04 [34] PDFs are slightly higher at small values of x and lower at large values of x than the AFG [35] PDFs, but the numerical difference is very small. In order to assess the potential of the ZEUS data [9] to constrain the photon PDFs, we also employ set GRV HO [36] by Glück, Reya, and Vogt, which we transform from the DIS_γ scheme to the $\overline{\text{MS}}$ scheme. For the $D^{*\pm}$ FFs, we use the parameterization of Ref. [6], where separate NLO fits to ALEPH and OPAL data are performed. As our default, we chose the set obtained from the fit to the OPAL data, as it has a lower χ^2 value. However, the differences in the considered cross sections resulting from exchanging the two FF sets are negligible. For

$\alpha_s^{(n_f)}(\mu)$, we use an exact solution of the two-loop renormalization group equation, where the asymptotic scale parameter $\Lambda^{(5)}$ for $n_f = 5$ is calculated from $\Lambda^{(4)}$ by requiring continuity of α_s at the bottom threshold $\mu = 2m_b$, and $\Lambda^{(4)}$ is set to 278 MeV to be consistent with the MRST03 [33] proton PDFs.

Our default scale choice is $\mu = m_T$ and $M = 2m_T$, where $m_T = \sqrt{m_c^2 + (p_T^D)^2}$ is the transverse mass of the $D^{*\pm}$ meson and we set $m_c = 1.5$ GeV. As usual, we identify the three factorization scales M_e , M_p , and M_F in Eq. (1) and denote their common value by M . In order to estimate the theoretical uncertainty in a conservative way, we vary μ and M independently about their default values, as $\mu = c_1 m_T$ and $M = 2c_2 m_T$ with $1/2 \leq c_1, c_2 \leq 2$. The maximum variation of the cross section thus obtained is shown as hatched green bands in Figs. 3–6. For comparison, we also consider *diagonal* scale variations, where $c_1 = c_2$, in these figures. However, we caution the reader that the errors resulting from diagonal scale variations are too optimistic because of cancellations due to the fact that the dependences of the cross section on μ and M act in opposite directions.

We chose the kinematics in such a way that a direct comparison to preliminary ZEUS data on $D^{*\pm}$ plus jet associated photoproduction [9] is possible. These data have been produced with a proton energy of 920 GeV and an electron energy of 27.5 GeV in the laboratory frame, which corresponds to a ep center-of-mass (c.m.) energy of $\sqrt{s} = 318$ GeV. The maximum photon virtuality is $Q_{\max}^2 = 1$ GeV², and the photon-proton c.m. energy W lies in the range $130 \text{ GeV} < W < 280 \text{ GeV}$. All rapidities η refer to the laboratory frame, with the HERA convention that the proton is moving towards positive rapidity. The jets are defined using the k_T -algorithm [37] with a jet radius of $R = 1$. We employ the ZEUS convention [9] that an event is counted twice if two jets in addition to the $D^{*\pm}$ meson are measured which both satisfy the cuts in transverse momentum and rapidity. However, we find that this case only occurs for about 0.3% of the generated events in the kinematic range considered. Unless stated otherwise, we adopt the acceptance cuts $p_T^D > 3$ GeV, $|\eta^D| < 1.5$, $p_T^j > 6$ GeV, and $-1.5 < \eta^j < 2.4$ from ZEUS [9]. We present histograms with the same binning as in Ref. [9]. As in Ref. [9], we consider the sum of the cross sections for D^{*+} and D^{*-} mesons.

We now present and discuss our figures. In Figs. 3–5, we confront the differential cross section of $ep \rightarrow D^{*\pm}j + X$ in photoproduction as measured by ZEUS [9] with our NLO predictions. Specifically, Fig. 3 refers to $d\sigma/dp_T^j$ integrated over the full η^j range ($-1.5 < \eta^j < 2.4$) and Figs. 4, 5(a) and (b) to $d\sigma/d\eta^j$ integrated over the full p_T^j range ($p_T^j > 6$ GeV)

and the subintervals $6 < p_T^j < 9$ GeV and $p_T^j > 9$ GeV, respectively. In addition, we present, in Figs. 6(a)–(d), $d\sigma/dp_T^j$ integrated over the subintervals $-1.5 < \eta^j < -0.5$, $-0.5 < \eta^j < 0.5$, $0.5 < \eta^j < 1.5$, and $1.5 < \eta^j < 2.4$, for which experimental data are not yet available. In all cases, the $D^{*\pm}$ meson is kinematically confined by the conditions $p_T^D > 3$ GeV and $|\eta^D| < 1.5$. The vertical bars on the ZEUS data [9] give the full errors, the purely statistical errors are indicated by the horizontal ticks on them. Our default predictions are represented by the solid red histograms and their errors due to independent scale variation by the hatched green bands. The errors due to diagonal scale variation are indicated by the dot-dashed and dotted pink histograms. The predictions evaluated for central scale choice with the GRV HO photon PDFs are given by the dashed blue histograms. We observe that our NLO predictions agree with the ZEUS data [9] within errors, except for two forward η^j bins in the lower p_T^j range, where the ZEUS data [9] slightly overshoot our NLO predictions. In the cases when the difference between the evaluations with the AFG04 [34] and GRV HO [36] photon PDFs is comparable to the experimental error, the GRV HO [36] set tends to yield a better description of the ZEUS data [9], except at large values of p_T^j and η^j .

It is also instructive to look at the distribution $d\sigma/dx_{\text{obs}}^\gamma$, where the kinematic observable x_{obs}^γ is defined as

$$x_{\text{obs}}^\gamma = \frac{p_T^D \exp(-\eta^D) + p_T^j \exp(-\eta^j)}{2E^\gamma}. \quad (4)$$

As the contribution from the direct-photon subprocesses peaks at $x_{\text{obs}}^\gamma \approx 1$, whereas resolved photons mainly contribute for $x_{\text{obs}}^\gamma < 1$, a cut on x_{obs}^γ can serve to obtain samples enriched in direct- or resolved-photon processes. As already mentioned in Sec.II, the true direct- and resolved-photon contributions are related at NLO through factorization and, taken separately, exhibit strong M_e dependences. Only their sum represents a physical observable that can be compared to experimental data. Notice that the individual parts can even be negative. In Fig. 7, our central NLO prediction for the differential cross section $d\sigma/dx_{\text{obs}}^\gamma$ in the kinematic range $p_T^D > 3$ GeV, $|\eta^D| < 1.5$, $p_T^j > 6$ GeV, and $-1.5 < \eta^j < 2.4$ (solid red histogram) is decomposed into its direct- (dashed blue histogram) and resolved-photon (dotted green histogram) components. We read off from Fig. 7 that, with our default scale choice, direct photoproduction dominates for $x_{\text{obs}}^\gamma \gtrsim 0.7$.

In the case of single-hadron inclusive photoproduction at HERA, the direct- and resolved-

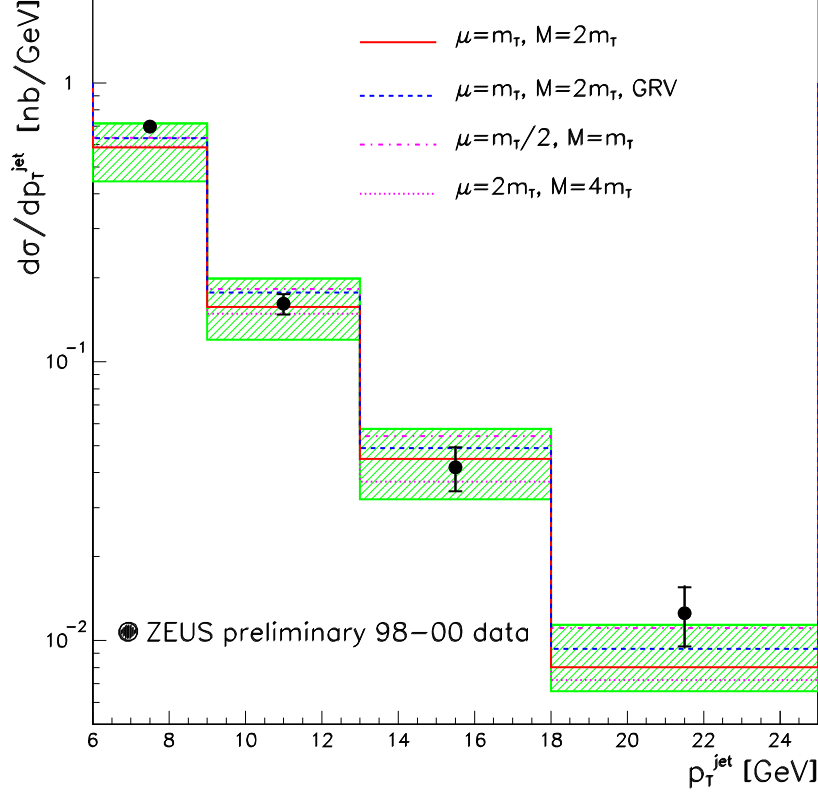


FIG. 3: The differential cross section $d\sigma/dp_T^j$ of $ep \rightarrow D^{*\pm}j + X$ in photoproduction for $-1.5 < \eta^j < 2.4$, $p_T^D > 3$ GeV, and $|\eta^D| < 1.5$ measured by ZEUS [9] is compared with our NLO predictions (solid red histogram) including conservative errors (hatched green bands). For comparison, the errors due to diagonal scale variation (dotted-dashed and dotted pink histograms) and the predictions evaluated for central scale choice with the GRV HO photon PDFs (dashed blue histogram) are also shown.

photon contributions are known to be accumulated in the backward and forward directions, respectively [38]. It is interesting to find out if, in $D^{*\pm}$ plus jet associated photoproduction, the rapidities η^D and η^j lend themselves as discriminators between direct and resolved photoproduction as well. To this end, we split our central NLO predictions for the differential cross sections $d\sigma/d\eta^j$ and $d\sigma/d\eta^D$ into their direct- and resolved-photon components and show the results in Figs. 8(a) and (b) as the solid red and dashed blue histograms, respectively. The kinematic range considered for $d\sigma/d\eta^j$ is $p_T^D > 3$ GeV, $|\eta^D| < 1.5$, and

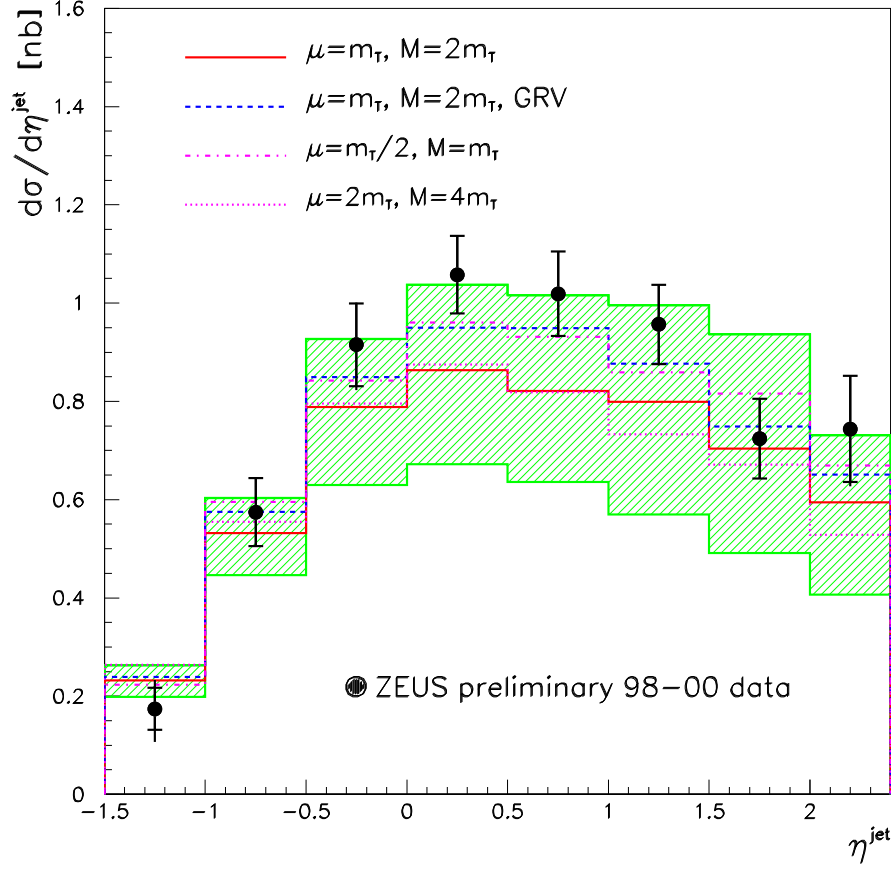


FIG. 4: Same as in Fig. 3, but for $d\sigma/d\eta^j$ with $p_T^j > 6$ GeV.

$p_T^j > 6$ GeV, while for $d\sigma/d\eta^D$ it is $p_T^D > 3$ GeV, $p_T^j > 6$ GeV, and $-1.5 < \eta^j < 2.4$. Notice that the superposition of the two histograms in Fig. 8(a) yields the solid histogram in Fig. 4. We learn from Figs. 8(a) and (b) that, in the kinematic range considered, the discriminating power of the rapidity distribution with respect to direct and resolved photons, which is familiar from single-hadron inclusive photoproduction at HERA, carries over to $d\sigma/d\eta^j$, but not to $d\sigma/d\eta^D$.

We now explore the sensitivity of our NLO predictions of $ep \rightarrow D^{*\pm}j + X$ in photoproduction to the gluon and charm-quark PDFs of the photon, so as to assess the potential of the HERA experiments to constrain these PDFs, which are presently less well known than those of the up, down, and strange quarks. In order to enhance this sensitivity, it is useful to suppress the direct-photon contribution. From the discussion of Figs. 7 and 8, we know

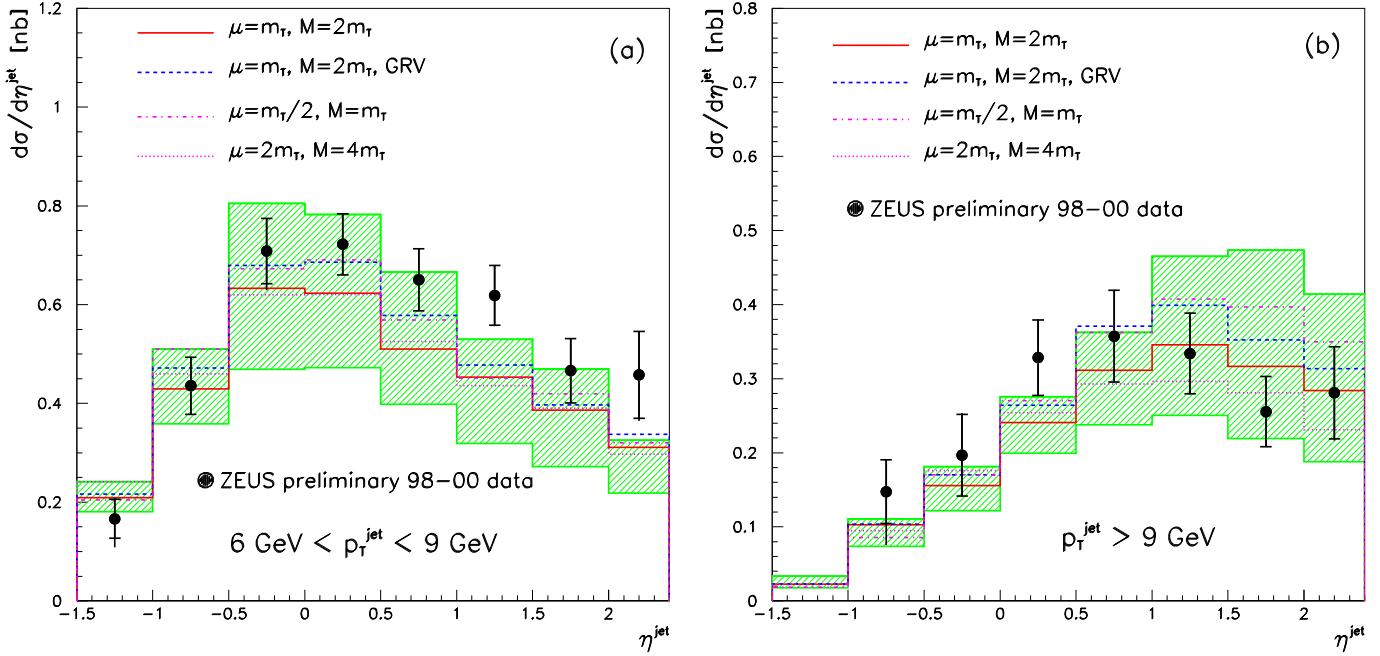


FIG. 5: Same as in Fig. 4, but for (a) $6 < p_T^j < 9$ GeV and (b) $p_T^j > 9$ GeV.

that this can be achieved by focusing on low values values of x_{obs}^γ and/or large values of η^j , typically $x_{\text{obs}}^\gamma \lesssim 0.75$ and $\eta^j \lesssim 0.5$. Therefore, we reconsider in Fig. 9 the differential cross section $d\sigma/d\eta^j$ for $p_T^D > 3$ GeV, $|\eta^D| < 1.5$, and $p_T^j > 6$ GeV (a) without and (b) with the acceptance cut $x_{\text{obs}}^\gamma < 0.75$ (solid blue histograms) and turn off the gluon (dashed red histograms) and charm-quark (dotted green histograms) PDFs, one at a time. Notice that the solid histograms in Figs. 4 and 9(a) are identical. We caution the reader that, strictly speaking, it is inconsistent to put to zero a photon PDF by hand because, in the determination of the PDF set, it participated in the DGLAP [13] evolution and thus influenced the other PDFs. Furthermore, its M_e dependence is correlated with a similar M_e dependence in the direct-photon contribution through the factorization procedure. Bearing these caveats in mind, it is nevertheless instructive to do so. We conclude from Fig. 9(a) and (b) that the contribution from the gluon inside the resolved photon is too small to be useful, while that from the charm quark is very significant. Quantitatively comparing Figs. 4, 8(a), and 9(a) after integration over η^j , we find that the contribution due to the charm component in the photon makes up 92% of the resolved-photon contribution and 50% of the total cross section. After imposing the condition $x_{\text{obs}}^\gamma < 0.75$, the latter fraction is increased to as much as 81%! In fact, the ZEUS data [9] in Fig. 4 overshoot the dotted green histogram in 9(a) by several experimental standard deviations in the upper η^j bins, which suggest that, in the framework of the ZMVFNS, the existence of intrinsic charm in the resolved photon is

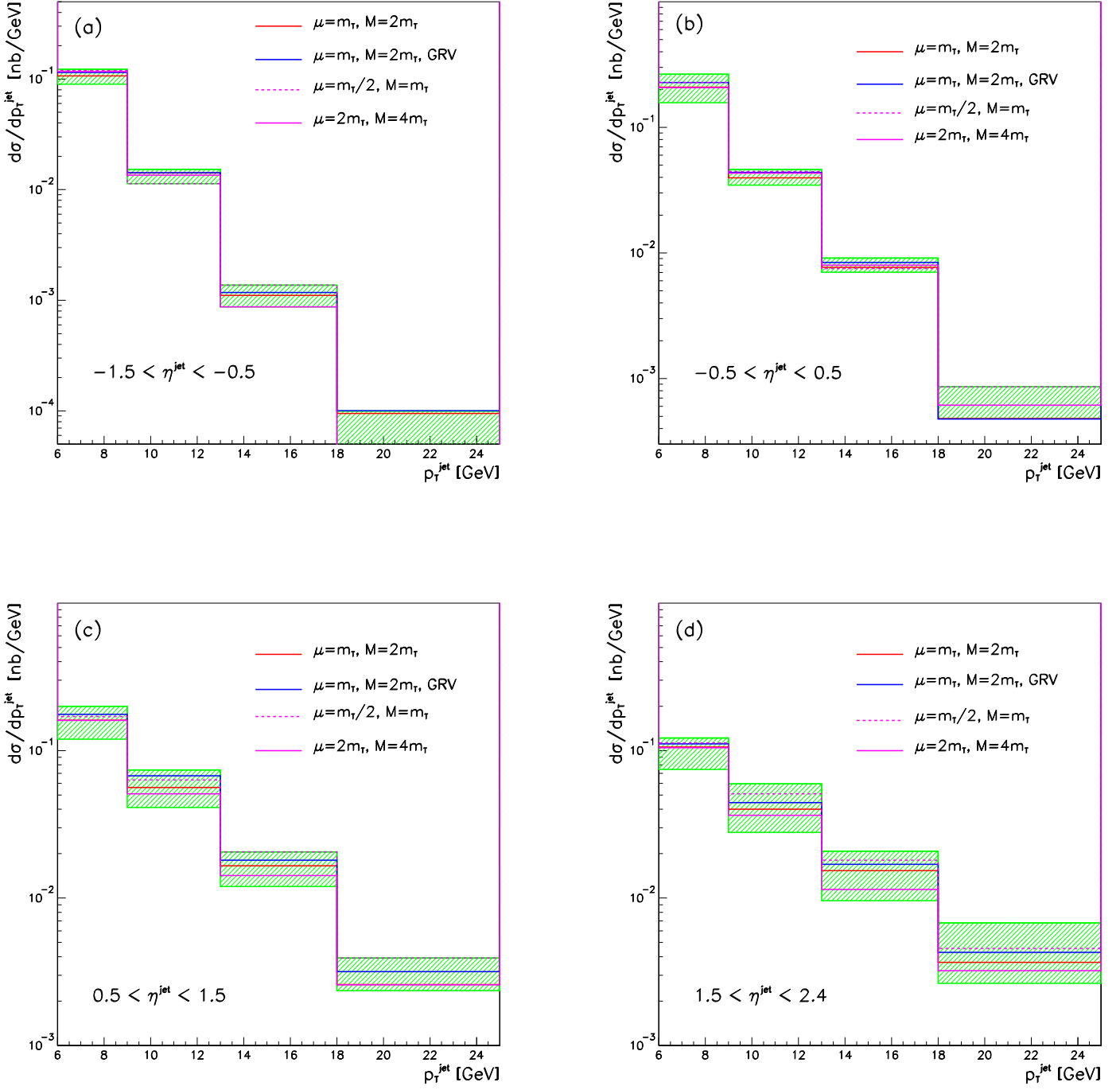


FIG. 6: Same as in Fig. 3, but for (a) $-1.5 < \eta^j < -0.5$, (b) $-0.5 < \eta^j < 0.5$, (c) $0.5 < \eta^j < 1.5$, and (d) $1.5 < \eta^j < 2.4$ and without experimental data.

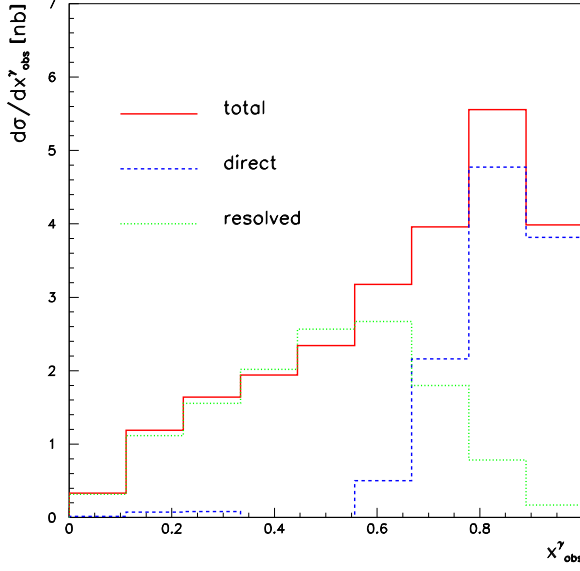


FIG. 7: Our central NLO prediction of the differential cross section $d\sigma/dx_{\text{obs}}^\gamma$ of $ep \rightarrow D^{*\pm}j + X$ in photoproduction for $p_T^D > 3$ GeV, $|\eta^D| < 1.5$, $p_T^j > 6$ GeV, and $-1.5 < \eta^j < 2.4$ (solid red histogram) and its direct- (dashed blue histogram) and resolved-photon (dotted green histogram) components.

experimentally established.

Another interesting observable is $\cos\theta^*$, defined as

$$\cos\theta^* = \tanh \frac{\eta^D - \eta^j}{2}. \quad (5)$$

As the angular dependence of subprocesses involving a gluon propagator in the t channel is approximately proportional to $(1 - |\cos\theta^*|)^{-2}$, whereas it is proportional to $(1 - |\cos\theta^*|)^{-1}$ in the case of a quark propagator, one can learn about the size of the contribution from diagrams of the type shown in Fig. 1(b) by studying the differential cross section $d\sigma/d\cos\theta^*$. A recent ZEUS analysis on dijet angular distributions in the photoproduction of open charm [7] has shown that the measured cross section from *resolved-enriched* events, with $x_{\text{obs}}^\gamma < 0.75$, exhibits a distinct asymmetry with a strong rise towards $\cos\theta^* = -1$, *i.e.*, the photon direction. This behaviour suggests that events with $x_{\text{obs}}^\gamma < 0.75$ are dominantly produced by charm quarks coming from the photon side. On the other hand, the $\cos\theta^*$ distribution for *direct-enriched* events, with $x_{\text{obs}}^\gamma > 0.75$, is almost symmetric, as expected for subprocesses like the one depicted in Fig. 1(a). In order to substantiate these observations from the theoretical side, we now investigate the differential cross section $d\sigma/d\cos\theta^*$ of $ep \rightarrow D^{*\pm}j + X$

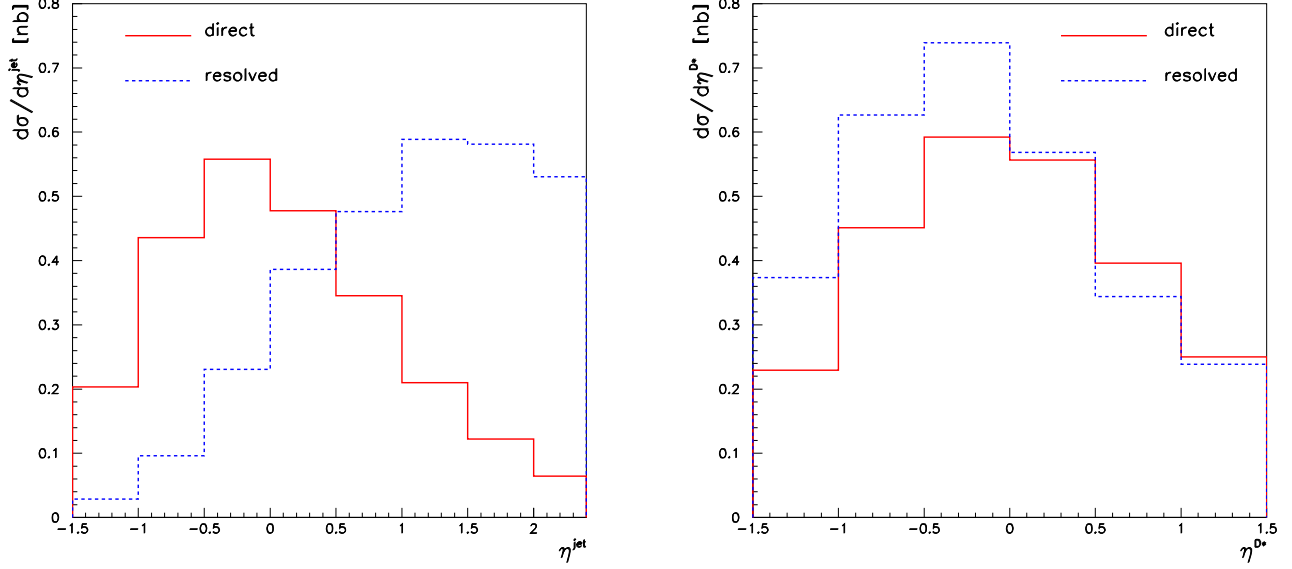


FIG. 8: Direct- (solid red histograms) and resolved-photon (dashed blue histograms) components of our central NLO predictions of the differential cross sections (a) $d\sigma/d\eta^j$ for $p_T^D > 3$ GeV, $|\eta^D| < 1.5$, and $p_T^j > 6$ GeV and (b) $d\sigma/d\eta^D$ for $p_T^D > 3$ GeV, $p_T^j > 6$ GeV, and $-1.5 < \eta^j < 2.4$ of $ep \rightarrow D^{\pm}j + X$ in photoproduction.

in photoproduction for $p_T^D > 3$ GeV, $|\eta^D| < 1.5$, $p_T^j > 6$ GeV, and $-1.5 < \eta^j < 2.4$ at NLO. In Fig. 10, this cross section is decomposed in two ways: in the physically well-defined direct- (dotted blue histogram) and resolved-enriched (solid red histogram) contributions, with $x_{\text{obs}}^\gamma > 0.75$ and $x_{\text{obs}}^\gamma < 0.75$, respectively; and in the mathematically defined direct- (dashed pink histogram) and resolved-photon (dot-dashed green histogram) contributions. From Fig. 10, we observe that the direct- and resolved-enriched contributions, which can be measured experimentally, exhibit very similar $\cos\theta^*$ dependences as their theoretical counterparts, which, taken separately, do not represent physical observables. In other words, the enriched contributions possess a rather high *purity*. Furthermore, we can confirm the findings of Ref. [7] concerning the $\cos\theta^*$ dependences of the direct- and resolved-enriched samples: the former is almost symmetric, whereas the latter exhibits a steep rise towards the photon direction. This demonstrates that the bulk of the resolved-photon contribution is due to charm component, in accordance with our conclusions from Figs. 9(a) and (b).

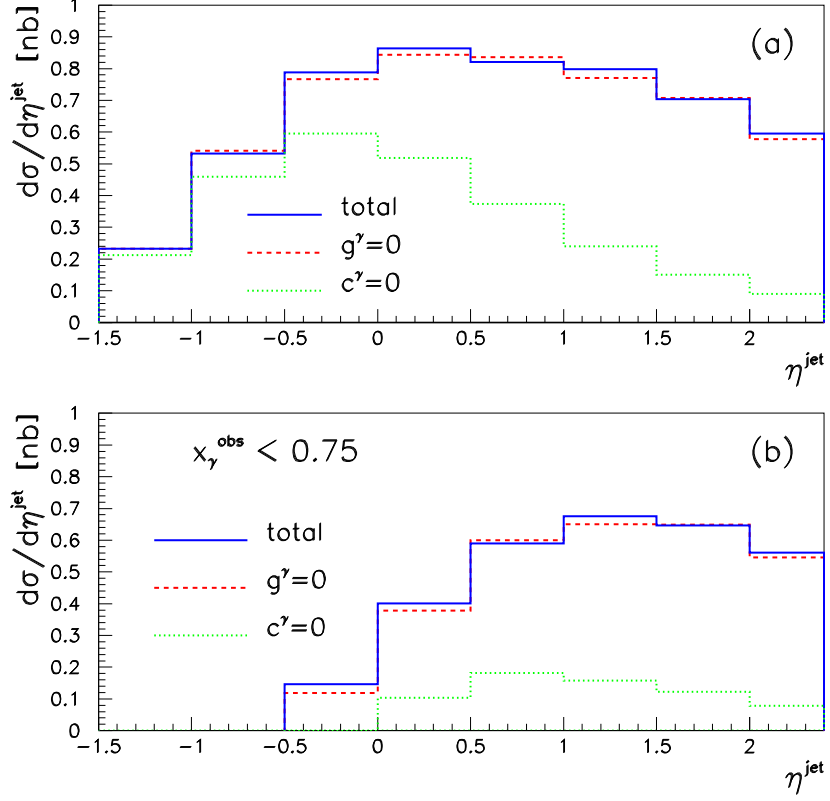


FIG. 9: Our central NLO prediction of the differential cross section $d\sigma/d\eta^j$ of $ep \rightarrow D^{*\pm}j + X$ in photoproduction for $p_T^D > 3$ GeV, $|\eta^D| < 1.5$, and $p_T^j > 6$ GeV (a) without and (b) with the acceptance cut $x_\gamma^{\text{obs}} < 0.75$ (solid blue histograms) and the evaluations with $F_{g/\gamma} = 0$ (dashed red histograms) or $F_{c/\gamma} = 0$ (dotted green histograms).

IV. CONCLUSIONS

Using results from Refs. [30, 32], we evaluated the cross section of $D^{*\pm}$ plus jet associated photoproduction at HERA to NLO in the parton model of QCD implemented in the ZMVFNS with non-perturbative FFs extracted from LEP1 [6], and studied various distributions of it. As the most important result, we found that preliminary ZEUS data [9] are nicely described by our theoretical predictions. This may be partly attributed to the fact that the acceptance cut $p_T^j > 6$ GeV [9] excludes events at energy scales of order m_c and below, which cannot be reliably described in this theoretical framework. In order to obtain a reliable prediction in the low- p_T range as well, the finite- m_c effects must be included, by working in the GMVFNS. In the case of $D^{*\pm}$ inclusive photoproduction, this

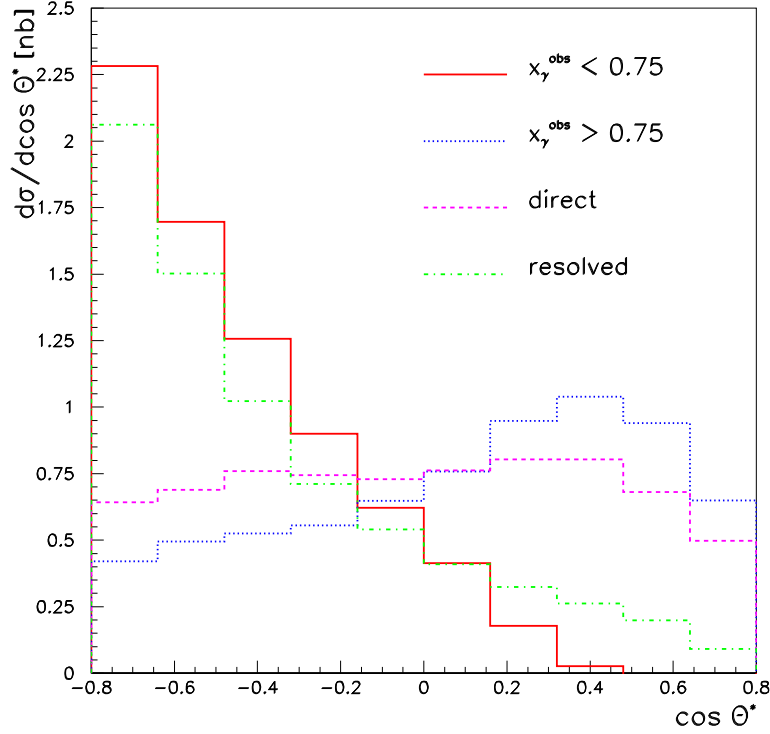


FIG. 10: Direct- (dashed pink histogram) and resolved-photon (dot-dashed green histogram) contributions as well as contributions with $x_{\text{obs}}^{\gamma} > 0.75$ (dotted blue histogram) and $x_{\text{obs}}^{\gamma} < 0.75$ (solid red histogram) to our central NLO prediction of the differential cross section $d\sigma/d\cos^*$ of $ep \rightarrow D^{*\pm}j + X$ in photoproduction for $p_T^D > 3$ GeV, $|\eta^D| < 1.5$, $p_T^j > 6$ GeV, and $-1.5 < \eta^j < 2.4$.

was recently done for the direct-photon contribution in Ref. [26]. The good agreement with the ZEUS data [9] provides successful tests of the universality and the scaling violations of the FFs, which are predicted by the factorization theorem and the DGLAP [13] evolution, respectively.

Unfortunately, the variation of the NLO predictions due to scale changes is larger than the one stemming from using different contemporary NLO sets of photon PDFs, so that the latter cannot be further constrained by measurements of $D^{*\pm}$ plus jet associated photoproduction at HERA.

As for the relative importance of the various partons inside the resolved photon, charm was found to greatly dominate, while the gluon turned out to be practically irrelevant. In

particular, the dominance of the charm component in the resolved photon manifests itself in the characteristic $\cos\theta^*$ dependence of the cross section, a feature that was already exploited in experimental analyses [7]. The comparison of the ZEUS data [9] with our NLO predictions establishes the presence of intrinsic charm inside the resolved photon with overwhelming significance and thus supports the validity and usefulness of the ZMVFNS endowed with non-perturbative FFs in the kinematic regime considered.

Acknowledgments

We would like to thank E. Gallo, L. Gladilin, J.H. Loizides, and F. Sefkow for helpful discussions about Refs. [3, 7, 8, 9, 10] and J.H. Loizides for making available to us the preliminary ZEUS data [9] in numerical form. B.A.K. thanks the Max-Planck-Institut für Physik for the hospitality extended to him during a visit when this work was finalized. This work was supported by the Bundesministerium für Bildung und Forschung through Grant No. 05 HT4GUA/4.

-
- [1] H1 Collaboration, S. Aid *et al.*, Nucl. Phys. **B472**, 32 (1996); H1 Collaboration, C. Adloff *et al.*, *ibid.* **B545**, 21 (1999).
 - [2] ZEUS Collaboration, J. Breitweg *et al.*, Phys. Lett. B **401**, 192 (1997).
 - [3] ZEUS Collaboration, J. Breitweg *et al.*, Eur. Phys. J. C **6**, 67 (1999).
 - [4] S. Frixione, M.L. Mangano, P. Nason, and G. Ridolfi, Nucl. Phys. **B412**, 225 (1994); Phys. Lett. B **348**, 633 (1995); S. Frixione, P. Nason, and G. Ridolfi, Nucl. Phys. **B454**, 3 (1995); S. Frixione and P. Nason, JHEP **0203**, 053 (2002).
 - [5] J. Binnewies, B.A. Kniehl, and G. Kramer, Z. Phys. C **76**, 677 (1997); M. Cacciari and M. Greco, Phys. Rev. D **55**, 7134 (1997); B.A. Kniehl, G. Kramer, and M. Spira, Z. Phys. C **76**, 689 (1997).
 - [6] J. Binnewies, B.A. Kniehl, and G. Kramer, Phys. Rev. D **58**, 014014 (1998).
 - [7] ZEUS Collaboration, S. Chekanov *et al.*, Phys. Lett. B **565**, 87 (2003); L. Gladilin, in *Proceedings of the XI International Workshop on Deep Inelastic Scattering (DIS 2003)*, St. Petersburg, Russia, 2003, edited by Victor T. Kim (World Scientific, Singapore, 2004), Report No.

- hep-ex/0309043; S. Padhi, PhD Thesis, McGill University, Montreal, Canada, 2003, Report No. DESY-THESIS-2004-012.
- [8] ZEUS Collaboration, T. Kohno for the collaboration, in *Proceedings of the XII International Workshop On Deep Inelastic Scattering (DIS 2004)*, Štrbské Pleso, Slovakia, 2004 (to appear); T. Kohno, KEK-REPORT-2004-3, 2004.
 - [9] ZEUS Collaboration, Abstracts 5-332 and 11-333, submitted to *32nd International Conference on High Energy Physics (ICHEP'04)*, Beijing, China, 2004.
 - [10] F. Sefkow, private communication; H1 Collaboration, in preparation.
 - [11] J. Binnewies, B.A. Kniehl, and G. Kramer, Z. Phys. C **65**, 471 (1995); Phys. Rev. D **52**, 4947 (1995); B.A. Kniehl, G. Kramer, and B. Pötter, Nucl. Phys. **B582**, 514 (2000); **B597**, 337 (2001); S. Kretzer, Phys. Rev. D **62**, 054001 (2000); L. Bourhis, M. Fontannaz, J.P. Guillet, and M. Werlen, Eur. Phys. J. C **19**, 89 (2001).
 - [12] J. Binnewies, B.A. Kniehl, and G. Kramer, Phys. Rev. D **58**, 034016 (1998).
 - [13] V.N. Gribov and L.N. Lipatov, Yad. Fiz. **15**, 781 (1972) [Sov. J. Nucl. Phys. **15**, 438 (1972)]; G. Altarelli and G. Parisi, Nucl. Phys. **B126**, 298 (1977); Yu.L. Dokshitser, Zh. Eksp. Teor. Fiz. **73**, 1216 (1977) [Sov. Phys. JETP **46**, 641 (1977)].
 - [14] J.C. Collins, Phys. Rev. D **58**, 094002 (1998); private communication.
 - [15] C. Peterson, D. Schlatter, I. Schmitt, and P.M. Zerwas, Phys. Rev. D **27**, 105 (1983).
 - [16] B. Mele and P. Nason, Phys. Lett. B **245**, 635 (1990); Nucl. Phys. **B361**, 626 (1991); J.P. Ma, *ibid.* **B506**, 329 (1997); K. Melnikov and A. Mitov, Phys. Rev. D **70**, 034027 (2004).
 - [17] M. Cacciari, M. Greco, S. Rolli, and A. Tanzini, Phys. Rev. D **55**, 2736 (1997).
 - [18] B.A. Kniehl, M. Krämer, G. Kramer, and M. Spira, Phys. Lett. B **356**, 539 (1995).
 - [19] M. Cacciari, M. Greco, B.A. Kniehl, M. Kramer, G. Kramer, and M. Spira, Nucl. Phys. **B466**, 173 (1996).
 - [20] M.A.G. Aivazis, J.C. Collins, F.I. Olness, and W.-K. Tung, Phys. Rev. D **50**, 3102 (1994); F.I. Olness, R.J. Scalise, and W.-K. Tung, *ibid.* **59**, 014506 (1999); A. Chuvakin, J. Smith, and W.L. van Neerven, *ibid.* **61**, 096004 (2000).
 - [21] S. Kretzer, H.L. Lai, F.I. Olness, and W.K. Tung, Phys. Rev. D **69**, 114005 (2004).
 - [22] M. Cacciari, M. Greco, and P. Nason, JHEP **9805**, 007 (1998); M. Cacciari, S. Frixione, and P. Nason, *ibid.* **0103**, 006 (2001); M. Cacciari and P. Nason, Phys. Rev. Lett. **89**, 122003 (2002).

- [23] B.A. Kniehl, in *Proceedings of the 14th Topical Conference on Hadron Collider Physics: Hadron Collider Physics 2002*, Karlsruhe, Germany, 2002, edited by M. Erdmann und Th. Müller (Springer, Berlin, 2003), p. 161, Report No. hep-ph/0211008; B.A. Kniehl and F. Sefkow, in *Proceedings of the XI International Workshop on Deep Inelastic Scattering (DIS 2003)*, St. Petersburg, Russia, 2003, edited by Victor T. Kim (World Scientific, Singapore, 2004), Report No. hep-ph/0312054.
- [24] G. Kramer and H. Spiesberger, *Eur. Phys. J. C* **22**, 289 (2001).
- [25] G. Kramer and H. Spiesberger, *Eur. Phys. J. C* **28**, 495 (2003).
- [26] G. Kramer and H. Spiesberger, Report No. MZ-TH/03-18 and hep-ph/0311062 (unpublished).
- [27] W.T. Giele and E.W.N. Glover, *Phys. Rev. D* **46**, 1980 (1992); W.T. Giele, E.W.N. Glover, and D.A. Kosower, *Nucl. Phys.* **B403**, 633 (1993).
- [28] S. Frixione, Z. Kunszt, and A. Signer, *Nucl. Phys.* **B467**, 399 (1996); S. Catani and M.H. Seymour, *ibid.* **B485**, 291 (1997); **B510**, 503(E) (1997).
- [29] P. Chiappetta, R. Fergani, and J.P. Guillet, *Z. Phys. C* **69**, 443 (1996); M. Fontannaz, J.P. Guillet, and G. Heinrich, *Eur. Phys. J. C* **21**, 303 (2001); **22**, 303 (2001); M. Fontannaz and G. Heinrich, *ibid.* **34**, 191 (2004).
- [30] M. Fontannaz, J.P. Guillet, and G. Heinrich, *Eur. Phys. J. C* **26**, 209 (2002).
- [31] P. Aurenche, A. Douiri, R. Baier, M. Fontannaz, and D. Schiff, *Z. Phys. C* **24**, 309 (1984); R.K. Ellis and J.C. Sexton, *Nucl. Phys.* **B269**, 445 (1986); P. Aurenche, R. Baier, A. Douiri, M. Fontannaz, and D. Schiff, *ibid.* **B286**, 553 (1987).
- [32] M. Fontannaz, J.P. Guillet, and G. Heinrich, the computer program can be downloaded from the URL http://wwwlapp.in2p3.fr/lapth/PHOX_FAMILY/main.html; see also Ref. [30].
- [33] A.D. Martin, R.G. Roberts, W.J. Stirling, and R.S. Thorne, in *Proceedings of the XI International Workshop on Deep Inelastic Scattering (DIS 2003)*, St. Petersburg, Russia, 2003, edited by Victor T. Kim (World Scientific, Singapore, 2004), Report No. IPPP/03/43, DCPT/03/86, Cavendish-HEP-2003/13, and hep-ph/0307262.
- [34] P. Aurenche, J.P. Guillet, and M. Fontannaz, private communication.
- [35] P. Aurenche, J.P. Guillet, and M. Fontannaz, *Z. Phys. C* **64**, 621 (1994).
- [36] M. Glück, E. Reya, and A. Vogt, *Phys. Rev. D* **45**, 3986 (1992); **46**, 1973 (1992).
- [37] S. Catani, Yu.L. Dokshitzer, M.H. Seymour, and B.R. Webber, *Nucl. Phys.* **B406**, 187 (1993); S.D. Ellis and D.E. Soper, *Phys. Rev. D* **48**, 3160 (1993).

- [38] F.M. Borzumati, B.A. Kniehl, and G. Kramer, Z. Phys. C **59**, 341 (1993); B.A. Kniehl and G. Kramer, *ibid.* **62**, 53 (1994).
- [39] The non-logarithmic corrections of relative order α_s are fully included, except for terms that are suppressed by powers of $\left(m_Q^2/\mu^2\right)^n$.